Multi-Axis Maglev Nanopositioner for Precision Manufacturing and Manipulation Applications

Shobhit Verma, *Student Member, IEEE*, Won-jong Kim, *Senior Member, IEEE*, and Huzefa Shakir, *Student Member, IEEE*

***Abstract*—We present a six-axis magnetic-levitation (maglev) stage capable of precision positioning down to several nanometers. This stage has a simple and compact mechanical structure advantageous to meet the performance requirements in the next-generation nanomanufacturing. It uses the minimum number of linear actuators required to generate all six axis motions. In this paper, we describe the electromechanical design, modeling, and control, and the electronic instrumentation to control this maglev system. The stage has a light moving-part mass of 0.2126 kg. It is capable of generating translation of 300 μm in the x, y, and z axes, and rotation of 3 mrad about the three orthogonal axes. The stage demonstrates position resolution better than 5 nm rms and position noise less than 2 nm rms. Experimental results presented in this paper show that the stage can carry, orient, and precisely position a payload as heavy as 0.4 kg. The pull-out force was found to be 8.08 N in the vertical direction. Furthermore, under a load variation of 0.14 N, the nanopositioner recovers its regulated position within 0.6 s. All these experimental results match quite closely with the calculated values because of the accurate plant model and robust controller design. This device can be used as a positioning stage for numerous applications, including photolithography for semiconductor manufacturing, microscopic scanning, fabrication and assembly of nanostructures, and microscale rapid prototyping.**

***Index Terms*—Lorentz-force linear actuator, magnetic levitation, permanent-magnet machine, precision motion control, system modeling and control.**

I. Introduction

POSITIONING stages have been used in the industry for various applications in machining, coordinate measuring, scanning for profile sensing, etc. The need of precision-positioning stages increased drastically due to their crucial role in the fabrication of micro and nanosized objects and assemblies. The key role of a nanopositioning stage is to load, position, and orient such an object and keep it stable without much vibration or noise. Most significant requirements for the actuators in nanomanipulation include accuracy, range of motion, degrees of freedom, and bandwidth [1].

Commonly used devices for micromanipulation are scanning tunneling microscopes (STMs) and atomic force microscopes (AFMs). Most of them are actuated by piezoelectric materials [2], [3]. However, there are certain challenges with the piezoelectric actuation systems: 1) the accuracy is greatly influenced by thermal drift under temperature variation; 2) the hysteresis in piezoelectric materials reduces the repeatability in positioning; and 3) a slow creeping motion after a large voltage step results in a significant positioning error [4]. The motion capability of these devices is usually limited to linear motions with a short travel range of around 100 μm.

For a long period of time researchers have been looking for solutions to single-axis or multi-axis nanopositioning. Egshira *et al.* developed a high-speed precision stage with a resolution of 0.69 nm using a nonresonant-type ultrasonic motor [5]. A high-bandwidth linear actuator capable of generating 1-nm steps without overshoot or undershoots was fabricated by Mori *et al.* [6]. Sun *et al.* demonstrated a dual-axis electrostatic microactuation system, which is capable of 0.01-μm resolution in 5-μm position change [7]. A high-stiffness linear piezoelectric motor with a resolution of 5 nm and output force of 200 N was presented by Zhang and Zhu [8].

The maglev technology has been successful for nanopositioning applications. The main benefit of magnetic levitation over other technologies is its noncontact nature while in operation, i.e., the forces are applied to the moving part without any mechanical contact. Since the moving part is levitated in the air, there is no friction, hysteresis, or backlash. Kim *et al.* constructed a six-degrees-of-freedom (6-DOF) high-precision planar maglev stage with large planar motion capability that had 10-nm position resolution and 100-Hz control bandwidth [9], [10]. Holmes *et al.* fabricated a maglev scanning stage with three-sigma horizontal position noise of 0.6 nm [11]. The stage utilizes four levitation linear motors to suspend and servo the moving element (platen) throughout its 25 mm $\times$ 25 mm $\times$ 0.1 mm range of travel. Position feedback is provided by three plane-mirror interferometers and three capacitance probes. The suspended platen (12-kg mass) is floated in oil to enhance the stage's disturbance rejection and to reduce power dissipation in the actuators. Jung and Baek designed and demonstrated a 6-DOF maglev positioner with self-stability for 5 DOFs [12]. It has a moving mass of 173 g with a position resolution of 0.5 μm in 32-mm-wide x–y planar motion and a 0.45-μm resolution in z motion.

Among the potential applications of this maglev nanopositioning device is the manufacture of small objects. This stage in conjunction with other manufacturing technologies that can provide with fabrication and assembly at microlevel will be able to produce microsized objects. In such applications this maglev stage will be used as the positioning device and the fabrication/scanning of parts can be done with a fixed tool. One

Paper IPCSD-05-052, presented at the 2004 Industry Applications Society Annual Meeting, Seattle, WA, October 3–7, and approved for publication in the IEEE TRANSACTIONS ON INDUSTRY APPLICATIONS by the Electric Machines Committee of the IEEE Industry Applications Society. Manuscript submitted for review August 20, 2004 and released for publication June 4, 2005. This work was supported by the National Science Foundation under Grant CMS-0116642.

The authors are with the Department of Mechanical Engineering, Texas A&M University, College Station, TX 77843-3123 USA (e-mail: shobhit.verma@gmail.com; wjkim@tamu.edu; huzefa@tamu.edu).

Digital Object Identifier 10.1109/TIA.2005.853374

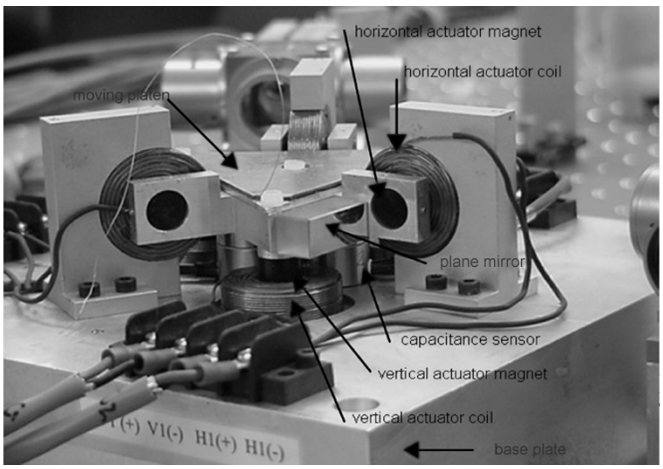

Fig. 1. Photograph of the nanopositioning maglev stage.

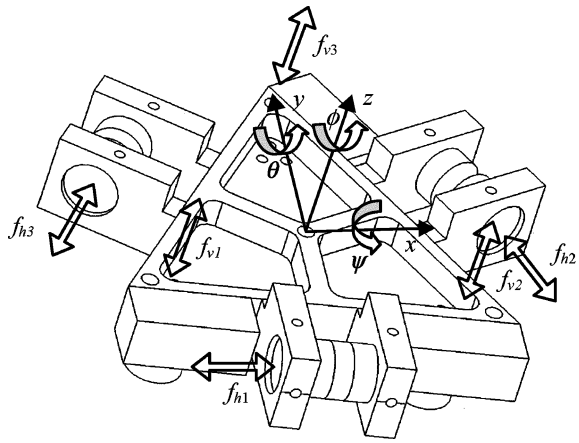

Fig. 2. Convention of the coordinate axes and the directions of forces generated by the unit linear actuators.

of such techniques is microstereolithography (μSTL). Classical STL processes use a laser beam deflected by a pair of low-inertia galvanometric mirrors and focused by a dynamic lens to solidify the polymer. This methodology works well for objects on the order of a few hundred micrometers. However, beam defocusing becomes problematic for smaller objects. An alternate approach is to keep the laser beam fixed and use a high-precision positioning stage for generating x–y motion for scanning [13]. Beluze *et al.* Zhang *et al.* and Jiang *et al.* have used this kind of x–y stages for μSTL [14]–[16]. Ikuta *et al.* showed the capability of such stages for the mass integrated harden polymer stereolithography process [17]. However, in all these processes, the minimum achievable part size is limited by the position resolution of the stage being used. In this paper, we demonstrate that this limitation in positioning can be easily overcome with our maglev stage.

In Section II, we present the mechanical design and assembly of the maglev stage, linear permanent-magnet unit actuators, and sensors and instrumentation system. Section III covers the plant modeling and control system design. This is followed by numerous experimental results in Section IV to demonstrate the performance of the stage under various payloads, abrupt load variations, and experimental verification of the pull-out force. In Section V, we show the precision motion capabilities of the maglev stage with the test results of generating a variety of single- and multiple-axis motion profiles. Finally, the need and utility of this research is summarized in Section VI with an emphasis on industrial applications.

II. 6-DOF Maglev Stage

A. Mechanical Design and Assembly

We developed a compact single-moving-part maglev stage. A photograph of the assembly is shown in Fig. 1. The moving-part assembly consists of a single-piece triangular aluminum platen pocket-milled to reduce the mass while maintaining the structural stiffness. There are three layers on the top of the platen, an aluminum top plate, a viscoelastic damping layer, and a stainless-steel constraint layer. The assembly of these three layers adds passive damping to the system to minimize structural vibration and improve stability. There is no ferromagnetic part in the assembly, which prevents iron loss and helps making the system controllable at high bandwidth. The mass of this platen assembly is just 0.2126 kg, and the total power consumption by all the actuators is only about a watt. There are three sets of arms protruded on the sides of the platen to hold six cylindrical permanent magnets for horizontal actuation. The other three magnets are attached on the bottom surface for vertical actuation. The coils for all six actuators are mounted on an aluminum base plate via coil holders. There are three plane mirrors attached to the sides of the platen for horizontal motion sensing. Vertical motion sensing is accomplished by three capacitance sensors mounted on the base plate right below the platen.

B. Linear Permanent-Magnet Unit Actuators

The six-axis motion generation by the platen is achieved by the application of six independent force components. The directions of the forces generated by the actuators are shown in Fig. 2. The magnitude of the force was calculated using the Lorentz force equation given as

$$\boldsymbol{f} = \int (\boldsymbol{J} \times \boldsymbol{B}) dV \tag{1}$$

where $\boldsymbol{J}$ is the current density in the coil and $\boldsymbol{B}$ is the magnetic flux density due to the permanent magnet. The axial force from the interaction of the current-carrying volume with the surface magnetic charges of the permanent magnet is

$$\begin{aligned} F_z(z) &= \left(\frac{J\mu_0(\mu_0 M)}{4\pi\mu_0}\right) \int_{c-\frac{w}{2}}^{c+\frac{w}{2}} \int_{Z-\frac{h}{2}}^{Z+\frac{h}{2}} \int_0^{2\pi} \frac{d}{dr} \\ &\quad \times \left[\int_0^R \int_0^{2\pi} \frac{\rho}{\sqrt{\left(z-\frac{d}{2}\right)^2 + r^2 + \rho^2 - 2r\rho\cos(\theta-\phi)}} d\theta d\rho \right. \\ &\quad \left. - \int_0^R \int_0^{2\pi} \frac{\rho}{\sqrt{\left(z+\frac{d}{2}\right)^2 + r^2 + \rho^2 - 2r\rho\cos(\theta-\phi)}} d\theta d\rho \right] \\ &\quad \times r d\phi dz dr \end{aligned} \tag{2}$$

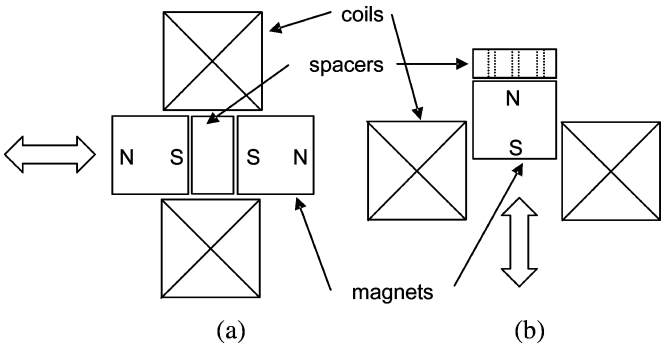

Fig. 3. (a) Horizontal and (b) vertical actuator units.

TABLE I
PROPERTIES OF PERMANENT MAGNET

Property	Value
diameter	11.7 mm
height	9.5 mm
material	NdFeB
energy product (BH_{max})	0.4 MJ/m^3 (50 MGOe)

TABLE II
PROPERTIES OF ACTUATOR COIL

Property	Value
wire guage	AWG#24
turns	179
resistance	0.6 Ω
inductance	0.5 mH
inner diameter	12.2 mm
outer diameter	32.5 mm
height	9.6 mm

where r is the radius and d is the height of the magnet, h is the height and w is the width of the coil, c is the average radius of the coil, and Z is the height of the center of the coil. The ρ and θ represent the coordinates of the small surface element of the magnet at the top and bottom surfaces in the cylindrical coordinates. The r, ϕ, and z represent the coordinates of the small volume element on the coil.

Each unit actuator consists of one coil epoxied to its coil holder and one or two magnets with their spacer or mount. The vertical actuators have one magnet, and the horizontal actuators have two magnets as shown in Fig. 3. There is a small spacer glued between the magnets in the horizontal actuator. The thickness, 4 mm, of this spacer was determined by the force equation (2) for maximum-force generation. We used cylindrical neodymium–iron–boron (NdFeB) magnets with the specifications given in Table I. The coils were wound with heavy-built copper magnet wire, and the specifications are given in Table II.

The current-carrying coil generates the N or S pole based on the direction of the current governed by the right-hand rule. Depending on its magnetization direction, an attractive or repulsive force is applied on the magnet. The reversal of the direction of the current will change the direction of the applied force. The precise assembly of the coils and magnets was a crucial task as the magnet–coil gap is just 0.5 mm, and a small error in assembly would lead to the reduction in the travel range. Thus, we designed and fabricated fixtures for precision assembly of the coils with their holders and the magnets with their spacers. The complete characterization of these actuators was described by Kim and Maheshwari [18].

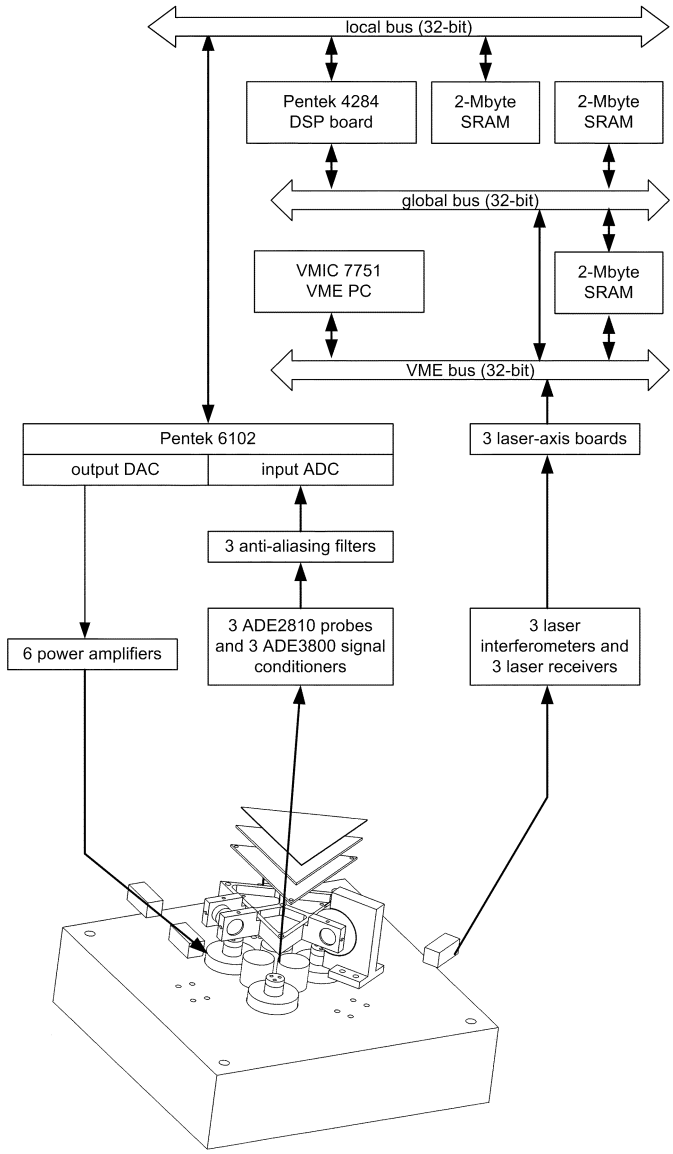

Fig. 4. Instrumentation structure.

The average nominal current in each vertical actuator is 0.7 A, so the nominal I^2R power consumption is 0.27 W in each actuator and 0.81 W in the whole actuation system to support the platen weight against the gravity. Most of the loss is joule loss because the stage has no ferromagnetic parts. The only part containing iron is the stainless-steel constraint layer far away (15–20 mm) from the coils, which makes iron loss negligible.

C. Sensors and Instrumentation System

The instrumentation structure is shown in Fig. 4. We use a VME (Versa Module Eurocard) chassis as a communication backbone among various electronics boards. This VME chassis has a VME PC (VMIC 7751), a digital signal processor (DSP)

board (Pentek 4284), a 16-bit data-acquisition board (Pentek 6102), and three laser-axis boards (Agilent 10 897B). The DSP board has a TMS320C40 DSP by Texas Instruments. It takes care of all the foreground computing tasks in real-time control. It gathers the position and velocity data from the laser-axis boards and the data-acquisition board, takes user commands or predefined positions and trajectories, applies the control law, calculates the control outputs, and generates the output commands via 16-bit digital-to-analog converters (DACs) also available on the Pentek 6102. All the above tasks are accomplished in an interrupt service routine (ISR) initiated by hardware interrupt at every 200 μs.

The actual position and velocity measurements of the platen are essential for real-time control. The three-axis position and velocity in the horizontal plane (x, y translation, and ϕ rotation) is sensed by laser interferometers with a resolution of 0.6 nm. The three plane mirrors mounted on the platen reflect the He–Ne laser beam, and the receivers give the raw data to the laser-axis boards for processing. The laser-axis boards output at 10-MHz 35-bit position and 24-bit velocity data that are received by the DSP via the VMEbus.

We use three capacitance gauges (ADE 2810) for vertical position sensing. These gauges face the bottom surface of the platen to sense its height at three different locations with an accuracy of 50 nm. With a triangulation method we calculate the z translation and ψ and θ rotations. The outputs of these gauges are fed to their signal conditioning boards (ADE 3800). The ADE 3800 boards give the analog signals corresponding to the platen position in the vertical axes. We sample the analog signals and convert them to digital data using 10-bit analog-to-digital converters (ADCs) on the Pentek 6102. These sensor data are used by the real-time digital controller. To avoid the aliasing of the sensor signals by higher frequency noise contents we use a set of first-order RC antialiasing filters with a cutoff frequency at approximately 1 kHz right before sampling by the ADCs.

The control outputs indicating desired coil currents are given to six transconductance amplifiers. The output current from an amplifier is linearly proportional to the input voltage. Each amplifier consists of a differential amplifier to reject common-mode noise, a feedback amplifier to stabilize the current-control loop, and a power booster with a power operational amplifier (PA12A) by Apex. These power amplifiers are connected to the coils to flow the commanded currents. The output swing of the DACs is ± 5 V and the current limit in the coils is set at ± 2.5 A.

III. System Modeling and Control

In this section, we present the modeling of the maglev stage. Then, a decoupled control strategy is discussed.

A. Plant Modeling

We built a three-dimensional (3-D) model of the whole maglev system with Solidworks and carried out mechanical finite-element analyses to identify various system parameters. The lowest natural frequency of the platen was found to be 4.6 kHz. Since the platen is magnetically levitated in the absence of any mechanical contact, the spring and damping effects are negligible. Thus, we model the platen as a pure mass, and the equation of motion for translation is

$$M\frac{d^2x}{dt^2} = f \tag{3}$$

where M is the mass of the platen, i.e., 0.2126 kg and f is the corresponding modal force. Thus, the transfer function of the platen for translation is

$$\frac{X(s)}{F(s)} = \frac{1}{0.2126s^2}. \tag{4}$$

Similarly, the transfer function of the platen for rotation is

$$\frac{\Theta(s)}{T(s)} = \frac{1}{Is^2} \tag{5}$$

where I is the moment of inertia about the corresponding axis. The values of principal moments of inertia I_{xx}, I_{yy}, and I_{zz} are 133×10^{-6}, 122×10^{-6}, and 236×10^{-6} kg $\cdot$ m^2, respectively.

B. Control System Design

Since the maglev system is open-loop unstable, a decoupled lead–lag controller was designed on the basis of the dynamic model derived in the previous section. The lag compensator with its pole placed at the origin eliminates the steady-state error and the lead compensator adds phase margin and damping. The controller was designed with damping ratio (ζ) of 0.7, and the phase margin of 50° at a crossover frequency of 48 Hz.

$$G(s) = K\frac{(s+130)(s+8)}{s(s+1130)} \tag{6}$$

where K is the gain of the controller that is calculated to keep the closed-loop characteristic equation the same for each axis. The calculated gains are 6.7897×10^4 N/m for x, y, and z translation. Since the moments of inertia about each axis are different, the gains for rotation are calculated as 42.438, 39.052, and 75.329 N for ψ, θ, and ϕ, respectively. We used the zeroth-order-hold (ZOH) equivalence method to convert this continuous-time controller to a discrete-time one with a 5-kHz sampling frequency and implemented it on the DSP as a difference equation.

IV. Load Tests

In this section, we present various load-test results to demonstrate the maglev stage's dynamic performance for nanomanufacturing and μSTL applications. In these applications, the positioner is supposed to carry small, but time-varying loads.

A. Pull-Out Force

We performed an experiment to determine the pull-out force of the maglev stage. We attached a spring at the center of the platen and applied a vertical force on it. The spring was pulled upwards manually, so the amount of the force was continuously increasing. Fig. 5 shows the platen position in z and the control effort f_z applied by the controller to maintain the platen position constant. The z-axis position of the platen shifted suddenly

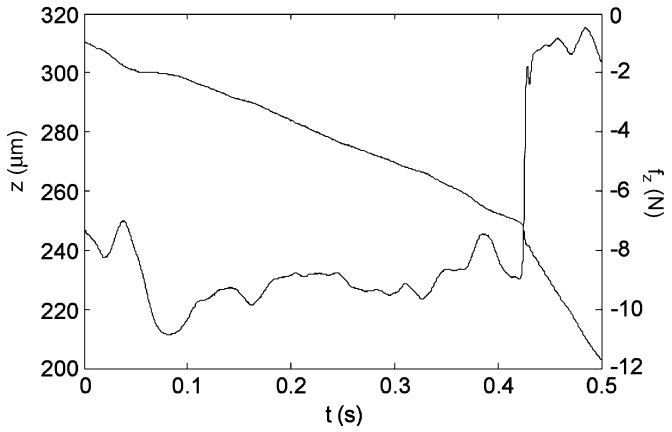

Fig. 5. Determination of the pull-out force with the vertical position z of the platen and the control effort f_z to maintain the platen position constant.

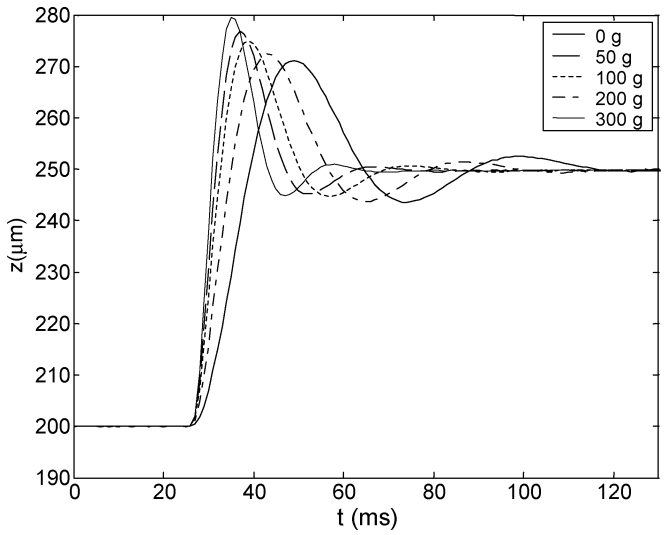

Fig. 6. No-load and load tests with 50-μm step responses in z with 0-, 50-, 100-, 200-, and 300-g added masses.

at around 0.425 s indicating the pull-out force of 7.75 N. The actuators are designed to deliver maximum current of 2.5 A with the force constant of 0.798 N/A. Thus, the maximum force that the controller can apply via the three vertical actuators to maintain the platen position would be 3×0.798 N/A $\times$ 2.5 A $=$ 5.99 N. Since the direction of the pull-out force is upwards, it balances the platen weight and then overcomes the vertical actuator forces. As the force to balance the weight of the platen is 0.2126 kg $\times$ 9.81 m/s^2 $=$ 2.09 N. The theoretical value of the pull-out force will be 5.99 N $+$ 2.09 N $=$ 8.08 N. The error in the experiment is only about 4%.

B. Step Responses with Various Payloads

To test the dynamic performance of the maglev stage, several step responses were taken with various payloads. The experimental results are shown in Fig. 6. The stage was able to levitate and position an additional mass of 0.4 kg on the platen. The payloads of more than 0.4 kg made the stage unstable due to actuator saturation in the overshoot. The additional payload increases the mass, keeping the system stiffness about the same, which decreases the natural frequency of the moving platen. Due to the lower natural frequency the rise time and the settling time are longer for the larger payloads as shown in the figure.

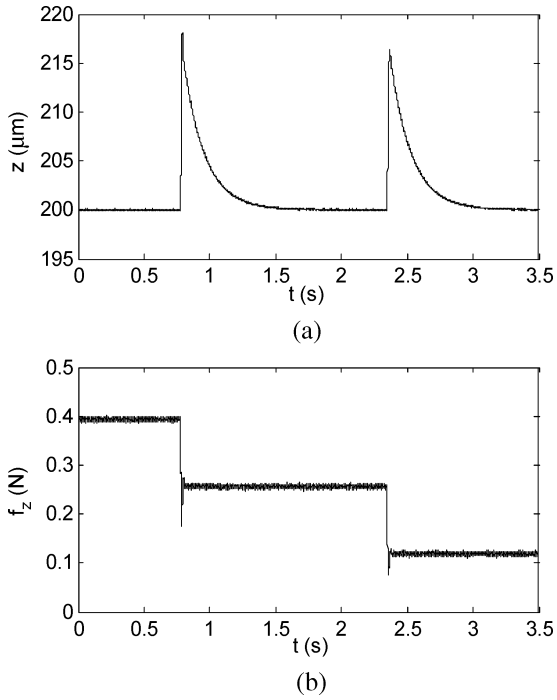

Fig. 7. (a) Position in z and (b) control effort f_z by the controller under sudden load changes. Each 14-g ceramic cylinder was removed at $t = 0.78$ and 2.35 s.

C. Recovery from Sudden Load Changes

To test the response of the platen for sudden load changes we placed small ceramic cylinders on the platen. We recorded the z-axis position and the control effort f_z by the controller to recover the position of the platen still under 6-axis magnetic levitation when the two ceramic cylinders were taken off. Fig. 7(a) shows the plot of the z-axis position, and Fig. 7(b) shows the control effort. The load removal occurred at 0.78 and 2.35 s, which generated perturbations in z. In the beginning of this experiment the vertical actuators were applying the forces precisely sufficient to balance the weight of the platen and the payload. As soon as the payload was removed, the applied force became greater than that to balance the weight of the platen and the payload. This excessive force gave the platen an instantaneous push upwards that was recovered by the controller over a period of 0.6 s. The maglev system's behavior was repeatable for the second load removal. It can be observed from Fig. 7(b) that the control effort in z decreased as soon as a ceramic cylinder was removed. The drop in the control effort was measured to be 0.14 N for first ceramic cylinder and 0.135 N for the second cylinder. The mass of each cylinder was 14 g, i.e., its weight is 0.137 N. This shows that the error between the experimental control effort and the actual force is only around 2%.

D. Recovery from Continuously Varying Load

We used a continuous flow of sand falling into a bowl placed on the platen to emulate the effect of the continuously varying load in nanomanufacturing and STL applications. The z position of the platen is shown in Fig. 8(a) and corresponding

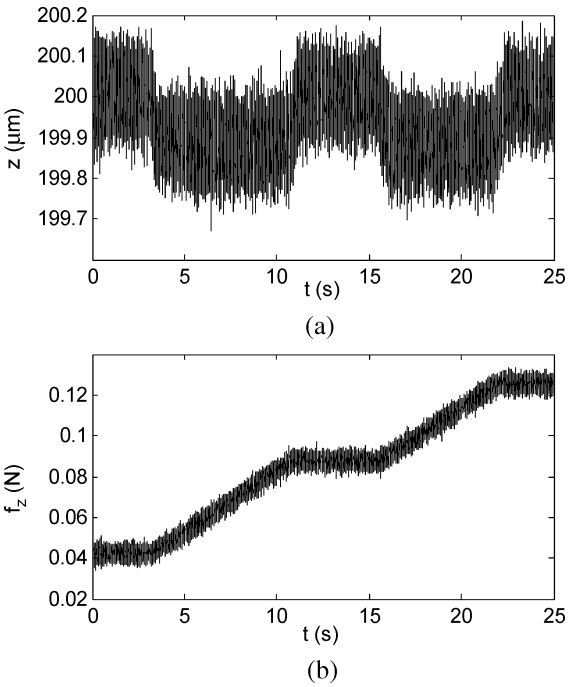

Fig. 8. (a) Position in z and (b) control effort f_z by the controller under continuously varying load.

required control effort is shown in Fig. 8(b). From the initial steady-state position of 200 μm, the mass inflow was initiated at 3 s and was stopped at 11 s, then started again at 16 s and stopped at 22 s. Since the rate of the mass change was almost constant, the control effort linearly increased to balance the additional mass on the platen and to regulate the vertical position of the platen at the same level. However, there was a small steady-state error in the vertical position during the mass variation, which acts like a constant force disturbance at the control input. This is attributed to the fact that the plant poles cannot be precisely located at the origin in the complex plane, and the controller was originally designed to meet the zero-steady-state error requirement for the position inputs with a single pole at the origin. Immediately after this disturbance was removed [between 11–15 s, and after 22 s in Fig. 8(a)], the steady-state error became zero, which demonstrates our controller's effectiveness and the fast closed-loop dynamics. The complete elimination of the steady-state error under the influence of the temporary constant disturbance is beyond the scope of this work.

V. Precision Motion Control

In addition to its load capacity demonstrated in the previous section, we present in this section the maglev stage's nanoscale multi-axis motion control capability.

A. Nanoscale Consecutive Steps

Fig. 9 shows the platen responses to 15-nm consecutive step commands at every 0.5-s time interval. The position repeatability is better than 2 nm. Fig. 9(b) and (c) shows the errors in x and y while generating these steps. The tracking error in x has peaks at every 0.5 s due to the abrupt changes in position. The regular noise level in x is close to 3 nm rms mainly due to these perturbations. The error in the y-axis is maintained below 2 nm rms. This shows that there is very little dynamic coupling between the x and y axes. In other words, no sudden change in x affects the y-axis motion, and the controller (6) is robust enough to keep the platen stable.

B. 100-nm Ramp Responses

In Fig. 10 the commanded path for the platen is an up-and-down ramp with the peak of 100 nm. Fig. 10(a) shows the actual path traversed by the platen. It is visible from the figure that the starting point of the trajectory is not exactly zero. This is due to nanoscale position noise in the stage. The peaks of the trajectory appear to be at around 105 nm and -5 nm instead of 100 nm and 0 nm because of the overshoots at the ends of the ramp trajectories. The path is more distorted near the ends due to the abrupt change in the direction of motion.

C. Two-Dimensional (2-D) Circular Motion

In our real-time control code written in C language, a set of data points in more than one axis can be allocated with respect to time so that the platen can follow a multi-axis trajectory. In Fig. 11(a), a commanded path of a 50-nm-radius circle and the response of the platen are shown. The trajectory errors in x and y in this nanoscale circular motion are shown in Fig. 11(b) and (c). We demonstrated that this maglev stage could follow nanoscale 2-D paths precisely.

D. 3-D Motion Generation for Micromanufacuring

We performed experiments to test the performance of the maglev stage with complex 3-D commanded paths. Among them a bowl-shaped trajectory with a parabolic vertical cross section is shown in Fig. 12. The platen closely followed the trajectory. The commanded point changed to make the platen move in a circular path by adding 1° rotation about the center at every sampling period of 200 μs.

Fig. 13 shows a 3-D trajectory followed by the platen layer by layer in the way as desired for μSTL to prove this maglev stage's positioning capability in micromanufacturing. The generated shape is of an impeller that has an outer radius of 25 μm and inner radius of 10 μm. The maglev stage was made to follow this whole 3-D motion trajectory in only 18 s, although the platen would need to be moved much slower in an actual μSTL process to allow sufficient time for the photopolymer to cure. These experimental results demonstrated the microscale 3-D motion-control capability of the maglev stage.

VI. Conclusions

Nanomanipulation has become essential for the development of nanotechnology. Nanopositioning stages that have high resolution in multiple axes with large travel ranges are in demand. In this paper, we presented the electromechanical design and control of a maglev stage as a promising solution for nanopositioning applications. This maglev stage has a simple mechanical structure without significant nonlinearity, which reduces the manufacturing cost and improves the dynamic performance. Its modeling and control system design were discussed in this paper. The dynamic performance of the system was demonstrated with various experiments.

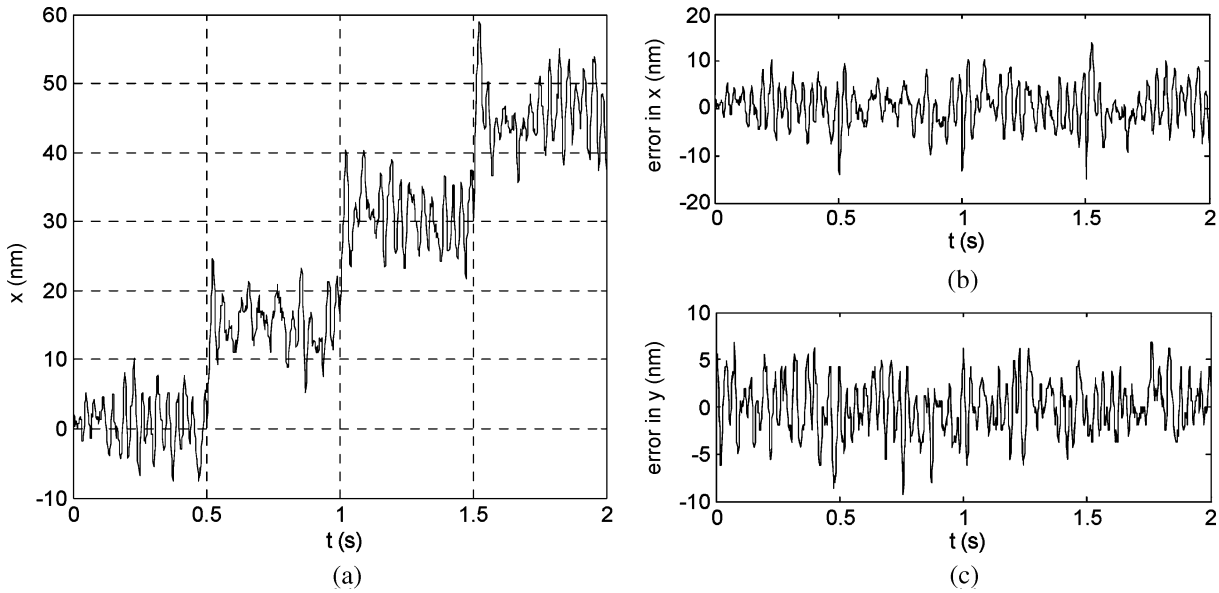

Fig. 9. (a) 15-nm consecutive steps at every 0.5-s time interval; (b) error in x and (c) error in y while generating these steps.

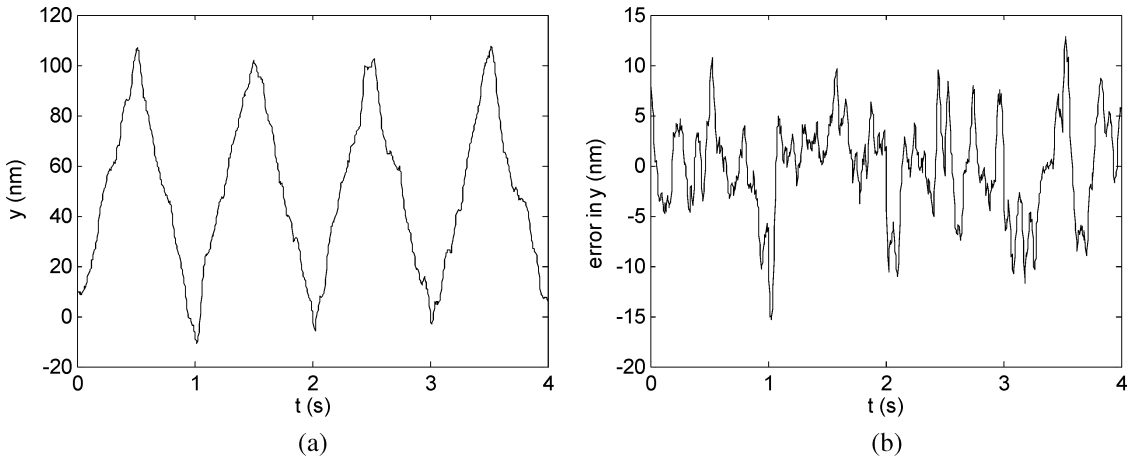

Fig. 10. (a) 100-nm up-and-down ramp response in y and (b) tracking error while the platen was following the commanded path.

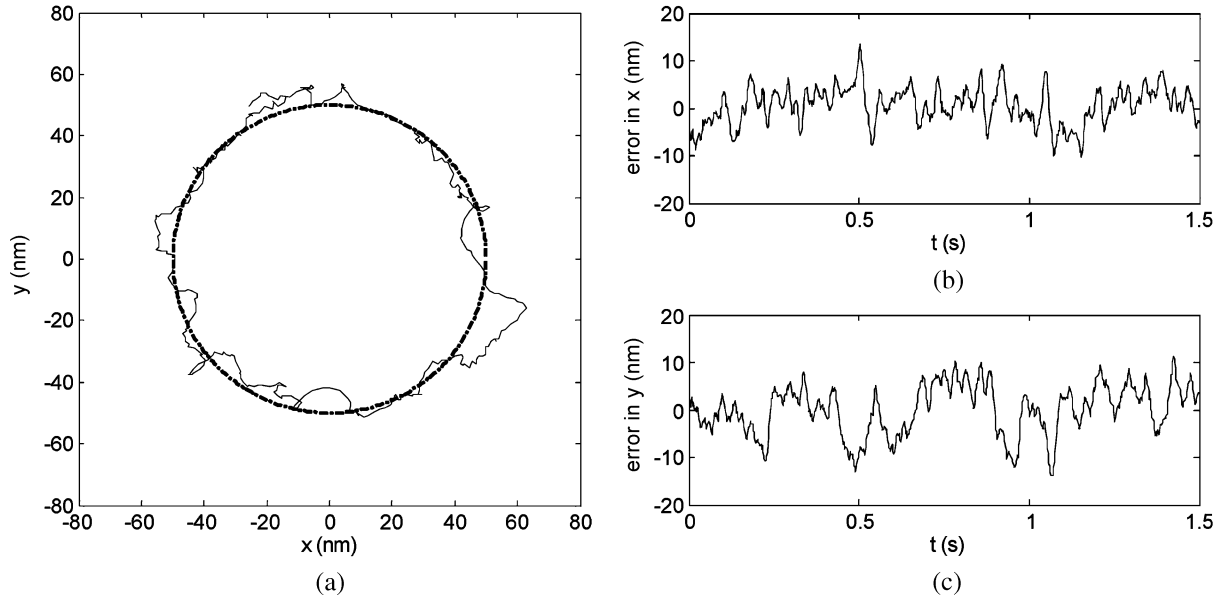

Fig. 11. (a) 50-nm-radius circle traversed in the x–y plane with commanded path and followed path; (b) error in x and (c) in y.

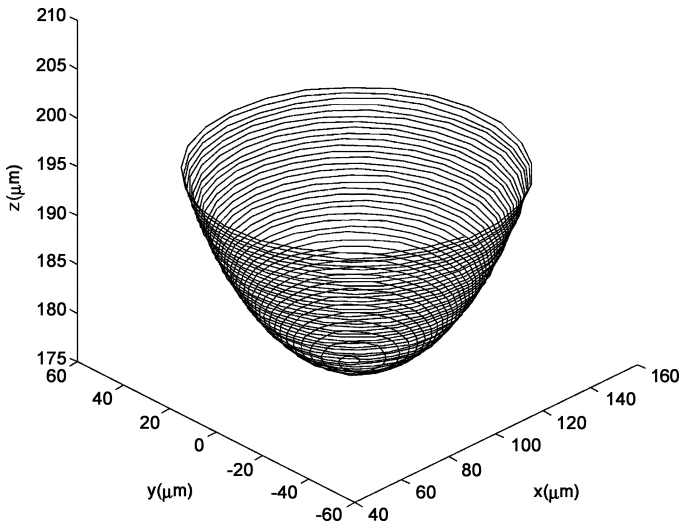

Fig. 12. A parabolic-shape bowl with a 20-μm height and 100-μm maximum radius traversed by the platen.

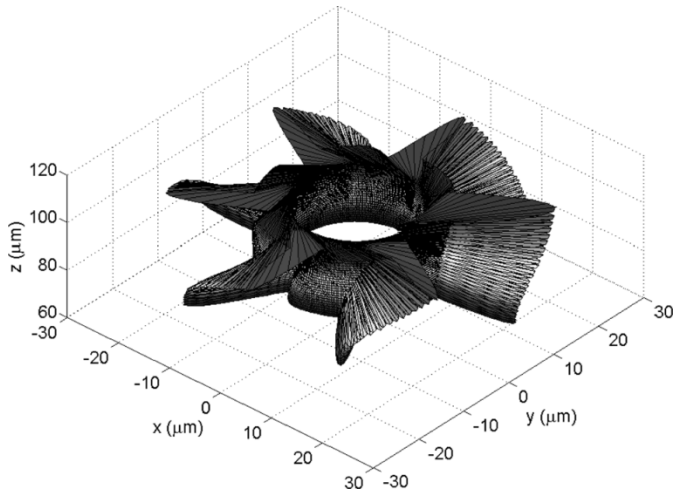

Fig. 13. A 3-D impelle shape traversed by the platen.

Step responses with different payloads showed that the derived plant model and the calculated parameters of the unit actuators such as their force constants were sufficiently accurate. The pull-out force was 7.75 N from experiments which matched closely with the calculated value of 8.08 N. Furthermore sudden changes in load did not make the system unstable, and the controller could recover a load variation of 0.14 N within 0.6 s and brought back the platen to the commanded position. In practical applications, the presence of external forces in the form of payload variation or mass fluctuation is inevitable. For instance, in μSTL, the mass of the substrate may vary as the photopolymer is solidified. Similarly, in microscanning applications, the load may vary in cantilever-probe-type scanning. Furthermore, there may be abrupt changes in external forces on the stage during contact mode operations. Apparently, in all these applications, the anticipated load variation is much less than the load capacity of the maglev stage demonstrated in Section IV. Thus, this stage guarantees a smooth vibration-free performance for the applications requiring precision positioning/scanning even in the presence of load fluctuations.

The platen was tested to track several one-dimensional, 2-D, and 3-D trajectories. These experimental results proved that this device was very successful in following complex paths with only nanometer-order tracking errors. This maglev stage that can generate complex multi-axis motions has numerous applications including ultrafine machining, precision positioning for scanning and characterization, manufacture of nanoscale structures, atomic-level manipulation, vibration isolation for delicate instruments, seismic motion detection, and microscale rapid prototyping.

ACKNOWLEDGMENT

The authors thank J. Gu for his contribution to design and software development.

REFERENCES

[1] M. Sitti, "Survey of nanomanipulation systems," in *Proc. IEEE NANO'01*, Oct. 2001, pp. 75–80.

[2] R. M. Taylor, "The nanomanipulator: A virtual reality interface to a scanning tunneling microscope," Ph.D. dissertation, Dept. Elect. Comput. Eng., Univ. North Carolina, Chapel Hill, NC, 1994.

[3] M. F. Yu, M. J. Dyer, H. W. Rohrs, X. K. Lu, K. D. Ausman, J. V. Her, and R. S. Ruoff, "Three-dimensional manipulation of carbon nanotubes under a scanning electron microscope," *Nanotechnology*, vol. 10, no. 3, pp. 244–252, Sep. 1999.

[4] A. A. G. Requicha, S. Meltzer, A. F. P. Terán, J. H. Makaliwe, H. Sikén, S. Hsieh, D. Lewis, B. E. Koel, and M. E. Thompson, "Manipulation of nanoscale components with the AFM: principles and applications," in *Proc. IEEE NANO'01*, Oct. 2001, pp. 81–86.

[5] Y. Egshira, K. Kosaka, S. Takada, T. Iwabuchi, T. Baba, S. Moriyama, T. Harada, K. Nagamoto, A. Nakada, H. Kubota, and T. Ohmi, "0.69 nm resolution ultrasonic motor for large stroke precision stage," in *Proc. IEEE NANO'01*, Oct. 2001, pp. 397–402.

[6] S. Mori, T. Hoshino, G. Obinata, and K. Ouchi, "Linear actuator with air bearing for highly precise tracking [HDD]," in *Dig. Asia-Pacific Magnetic Recording Conf.*, May 2002, pp. AP4-01–AP4-02.

[7] Y. Sun, D. Piyabongkarn, A. Sezen, B. J. Nelson, R. Rajamani, R. Schoch, and D. P. Potasek, "A novel dual-axis electrostatic microactuation system for macromanipulation," in *Proc. IEEE/RSJ Int. Conf. Intelligent Robots and Systems*, Oct. 2002, pp. 1796–1801.

[8] B. Zhang and Z. Zhu, "Developing a linear piezomotor with nanometer resolution and high stiffness," *IEEE/ASME Trans. Mechatronics*, vol. 2, no. 1, pp. 22–29, Mar. 1997.

[9] W.-J. Kim, "High-precision planar magnetic levitation," Ph.D. dissertation, Dept. Elect. Eng. Comput. Sci., Mass. Inst. Technol., Cambridge, MA, June 1997.

[10] W.-J. Kim and D. L. Trumper, "High-precision magnetic levitation stage for photolithography," *Precision Eng.*, vol. 22, no. 2, pp. 66–77, Apr. 1998.

[11] M. Holmes, R. Hocken, and D. L. Trumper, "The long-range scanning stage: a novel platform for scanned-probe microscopy," *Precision Eng.*, vol. 24, no. 3, pp. 191–209, Jul. 2000.

[12] K. S. Jung and Y. S. Baek, "Study on a novel contact-free planar system using direct drive DC coils and permanent magnets," *IEEE/ASME Trans. Mechatronics*, vol. 2, no. 1, pp. 35–43, Mar. 2002.

[13] V. K. Vardan, X. Jiang, and V. V. Vardan, *Microstereolithography and Other Fabrication Techniques for 3D MEMS*. Chichester, U.K.: Wiley, 2001, pp. 111–127.

[14] L. Beluze, A. Bertsch, and P. Renaud, "Microstereolithography: a new process to build complex 3D objects," in *Proc. SPIE*, vol. 3680, Apr. 1999, pp. 808–817.

[15] X. Zhang, X. N. Jiang, and C. Sun, "Microstereolithography of polymeric and ceramic microstructures," *Sens. Actuators A, Phys.*, vol. A77, no. 2, pp. 149–156, Mar. 1999.

[16] X. N. Jiang, C. Sun, X. Zhang, B. Xu, and Y. H. Ye, "Microstereolithography of lead zirconate titanate thick film on silicon substrate," *Sens. Actuators A, Phys.*, vol. A87, no. 1–2, pp. 72–77, May 2000.

[17] K. Ikuta, S. Maruo, and S. Kojima, "New microstereolithography for freely movable 3D microstructure-super IH process with submicron resolution," in *Proc. IEEE MEMS'98*, Jan. 1998, pp. 290–295.

[18] W.-J. Kim and H. Maheshwari, "High-precision control of a maglev linear actuator with nano-positioning capability," in *Proc. Amer. Control Conf.*, May 2002, pp. 4279–4284.

Shobhit Verma (S'02) received the B.Tech. degree in mechanical engineering and the M.Tech degree in computer integrated manufacturing from the Indian Institute of Technology, Bombay, India, in 2002. He is currently working toward the Ph.D. degree in the Department of Mechanical Engineering, Texas A&M University, College Station, in 2005.

He was a summer trainee with Crompton Greaves, India, in 2000. His research interests are magnetic levitation, precision positioning, and nanofabrication.

Mr. Verma is a Student Member of the American Society of Mechanical Engineers. He was the leading member of the winning team for Region XIII (outside North America) in the ASME Student Design Contest in 2000. In 2001, his team again represented Region XIII and was ranked fifth in the international finals during the ASME Conference held in New York.

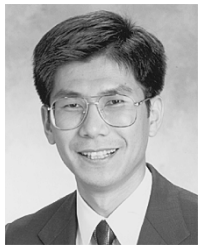

Won-jong Kim (S'89–M'97–SM'03) received the B.S. (*summa cum laude*) and M.S. degrees in control and instrumentation engineering from Seoul National University, Seoul, Korea, in 1989 and 1991, respectively, and the Ph.D. degree in electrical engineering and computer science from Massachusetts Institute of Technology (MIT), Cambridge, in 1997.

In September 2000, he joined the Department of Mechanical Engineering, Texas A&M University (TAMU), College Station, where he is currently an Assistant Professor. Following receipt of the Ph.D. degree, he was with SatCon Technology Corporation, Cambridge, MA, for three years. His teaching and research interests focus on analysis, design, and real-time control of mechatronic systems, networked control systems, and nanoscale engineering and technology. He is the holder of three U.S. patents on precision positioning systems.

Dr. Kim received the Grand Prize from the Korean Institute of Electrical Engineers' Student Paper Contest in 1988. His 1997 MIT dissertation earned him the Gold Prize from Samsung Electronics' Humantech Thesis Prize. He was a semifinalist in the NIST's Advanced Technology Program 2000 Competition. The NASA granted him the Space Act Award in July 2002. He was appointed a Select Young Faculty Fellow by TAMU College of Engineering and the Texas Engineering Experiment Station in September 2003. He is the Chair of the American Society of Mechanical Engineers (ASME) Nanoscale Control Technical Panel and a member of the IEEE Nanotechnology Council. He is a Member of the ASME, American Society for Precision Engineering, Korean-American Scientists-Engineers Association, Pi Tau Sigma, and Sigma Xi.

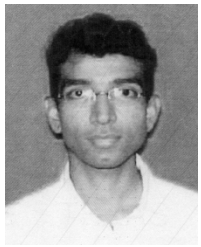

Huzefa Shakir (S'02) was born in Ujjain, India, in 1978. He received the B.Tech. (Honors) degree in mechanical engineering from the Indian Institute of Technology, Kharagpur, India, in 2000. He is currently working toward the Ph.D. degree at Texas A&M University, College Station.

In September 2002, he joined the Precision Mechatronics and Nanotechnology Laboratory, Department of Mechanical Engineering, Texas A&M University, where he is currently a Research Assistant. He was also a Teaching Assistant for one year for the Dynamic Systems and Controls and Engineering Dynamics courses. He was an Assistant Manager with Maruti Udyog Limited, India, a leading automobile manufacturing company, for two years following receipt of the undergraduate degree. His research interests include analysis and design of control systems and nanoscale manufacturing and motion control.

Mr. Shakir is a Student Member of the American Society of Mechanical Engineers and Phi Kappa Phi.